NASA TECHNICAL MEMORANDUM

NASA TM X-3443

NASA TM X-3443

METHOD OF DISCRETE MODELING AND ITS APPLICATION TO ESTIMATION OF TF30 ENGINE VARIABLES

Dale J. Arpasi and William M. Bruton

Lewis Research Center
Cleveland, Ohio 44135

NATIONAL AERONAUTICS AND SPACE ADMINISTRATION • WASHINGTON, D. C. • OCTOBER 1976

1. Report No. NASA TM X-3443	2. Government Accession No.	3. Recipient's Catalog No.
4. Title and Subtitle METHOD OF DISCRETE MODELING AND ITS APPLICATION TO ESTIMATION OF TF30 ENGINE VARIABLES		5. Report Date October 1976 6. Performing Organization Code
7. Author(s) Dale J. Arpasi and William M. Bruton		8. Performing Organization Report No. E-8560 10. Work Unit No. 505-05
9. Performing Organization Name and Address Lewis Research Center National Aeronautics and Space Administration Cleveland, Ohio 44135		11. Contract or Grant No. 13. Type of Report and Period Covered Technical Memorandum
12. Sponsoring Agency Name and Address National Aeronautics and Space Administration Washington, D.C. 20546		14. Sponsoring Agency Code
15. Supplementary Notes		

16. Abstract

A method of discrete modeling is presented that effectively isolates steady-state model accuracy from dynamic model accuracy. The steady-state model may be generated from the engine design equations with any desired degree of accuracy. The dynamic model is generated by applying a step disturbance of a manipulated variable to an open-loop engine simulation. The sampled response of the variable is combined with the steady-state model's response to form a set of weighting factors. These weighting factors are then used to weight past values of the manipulated variable, thus forming the dynamic model. The method is used to estimate various TF30-P-3 engine variables. A dynamic trim function is developed to compensate for the dynamic nonlinearities of the variables as well as for inaccuracies in dynamic definition. The trim function is shown to be related to the square root of the sum of the squares of the weighting factors obtained at various engine operating conditions. Finally, the estimation of variables without dynamic modeling is discussed.

17. Key Words (Suggested by Author(s))	18. Distribution Statement
Control Gas turbines Digital computers	Unclassified - unlimited STAR Category 07

19. Security Classif. (of this report)	20. Security Classif. (of this page)	21. No. of Pages	22. Price*
Unclassified	Unclassified	39	$4.00

* For sale by the National Technical Information Service, Springfield, Virginia 22161

METHOD OF DISCRETE MODELING AND ITS APPLICATION TO ESTIMATION OF TF30 ENGINE VARIABLES

by Dale J. Arpasi and William M. Bruton

Lewis Research Center

SUMMARY

A method of discrete modeling is presented that effectively isolates steady-state model accuracy from dynamic model accuracy. It is formulated so as to allow the inclusion of readily available steady-state engine relations to achieve any degree of steady-state modeling accuracy desired. A dynamic model based on the impulse transfer function may then be incorporated without affecting steady-state modeling accuracy.

The dynamic model is generated by applying a step disturbance of a manipulated variable to an open-loop engine simulation. The response of a particular engine variable of interest is sampled at a fixed interval to form a set of weighting factors that represent the dynamic response of the variable about an operating point. These factors are then used to accumulatively weight the past values of the derivative of the manipulated variable. The summation is multiplied by a simple trim function to account for dynamic variations due to changes in operating point. The resultant dynamic model is summed with the steady-state model to form the complete discrete model.

The model was applied to the estimation of the corrected low-pressure-compressor rotor speed, turbine-inlet temperature, and corrected airflow of both compressors in the TF30-P-3 turbofan engine. These estimates were formed for three different configurations of the steady-state model by using the derivative of corrected main-combustor fuel flow as the argument of the dynamic model. The dynamic model was generated from weighting factors obtained at a single operating point. A straight-line function of high-pressure-compressor rotor speed was chosen to modify the model dynamics for operation at other operating points. Each estimate was evaluated against its actual counterpart in the engine simulation for a step in throttle position from a subidle setting to the full augmentation setting of power-level position while the simulation was operating under the engine's bill-of-material control system.

INTRODUCTION

Airbreathing engine control requires the close regulation of certain engine variables to provide performance without violating engine operational limits. This regulation can be accomplished directly by the controller if these variables can be measured. However, the significant variables are not directly measurable. Sensors for these desired measurements are often unavailable for either technical or economic considerations. Consequently, the control engineer is forced to devise either a method of indirect regulation of these variables or an accurate means of estimating these variables to permit direct regulation in the control.

Presently, because accurate estimates are difficult to obtain, indirect regulation of unmeasurable variables is the common practice. Indirect regulation is normally accomplished by imposing limits on the manipulated variables (e.g., the acceleration limit schedule used in the main fuel controls). These limits are not easily defined in terms of the actual limit requirements of the unmeasurable variables (e.g., compressor surge and turbine overtemperature limits) and also are not easily modified for engine-to-engine variation and engine deterioration.

Variable estimation as an alternative to indirect regulation is enhanced by the trend toward incorporating sophisticated digital computers into the engine control loop. The computational power and memory capability of the computer permits storage of a mathematical model of the engine. This model would be capable of providing indirect observations of important engine variables based on the actual measurement of other engine variables. The indirect observation or estimate of these variables would then be incorporated with some control law for direct regulation.

This report describes a method of mathematical modeling that is particularly well suited to digital engine control. The method is based on the impulse transfer function and is formulated completely in the discrete time domain. Consequently, the model may be formed empirically by a digital computer directly monitoring an engine simulation or a well-instrumented prototype of the engine. In this case the models are determined by a digital computer from an extensive hybrid simulation of the engine. After a discussion of the general mathematical formulation of the model and certain practical considerations, the method of modeling is demonstrated by using it to provide estimates of various variables in the TF30-P-3 turbofan engine.

TF30-P-3 ENGINE DESCRIPTION

The Pratt & Whitney TF30-P-3 engine (fig. 1) is an axial, mixed-flow, augmented, twin-spool, low-bypass-ratio turbofan. A single inlet is used for both the fan airflow and the engine core airflow. Airflow leaving the fan is separated into two flow streams: one

stream passing through the engine core, and the other stream passing through the annular fan duct. A nine-stage, low-pressure compressor (LPC) includes the core portion of the three-stage fan and is connected by a throughshaft to the three-stage, low-pressure turbine. A seven-stage, high-pressure compressor (HPC) is connected by a hollow shaft to the single-stage, high-pressure turbine. A seventh-stage LPC bleed system discharges air into the fan duct at flight Mach numbers above 1.75. A twelfth-stage HPC bleed system automatically discharges air into the fan duct for compressor surge control. In the combustor, airflow from the compressors reacts with the injected fuel, producing high-energy gas to power the turbines.

The engine core and fan duct flow streams combine in an augmentor and are discharged through a variable-area convergent nozzle. The augmentor consists of a diffuser section and a combustion chamber. The fuel is introduced into the combustion chamber through spray rings that are arranged into five separate zones.

The bill-of-material control (BOM) of the TF30-P-3 engine is used to provide transient evaluation of the estimator models and is described in reference 1. The control provides regulation of the main-combustor fuel flow, the twelfth-stage compressor bleed, the variable exhaust nozzle, and the fuel flow to the five augmentor zones.

SIMULATION AND ESTIMATION APPARATUS

The simulation of the TF30-P-3 engine is detailed in reference 2. The equations describing the engine were implemented by using the Lewis Research Center's Analog and Hybrid Computing Facility. The Lewis EAI Model 690 Hybrid Computing System was used in conjunction with two EAI 231-R Analog Computers.

The bill-of-material control, the formulation procedure of the estimator models, and the estimator models were programmed on a general-purpose digital control system also located in this facility. This system uses an SEL 810B digital computer and is described in reference 3. Table I summarizes the capabilities of the digital control system.

MATHEMATICAL MODEL FORMULATION

In applying impulse response to model development, it was assumed that the engine is a single-input, multiple-output system with the relation between input and output being governed by external conditions. It was also assumed that measurement of the engine variable to be modeled is available (as from a simulation of the engine) even though in actuality that variable is unmeasurable.

Accuracy problems involved with direct application of the impulse transfer function to model development are indicated and thus an alternative form, making use of a separately evolved steady-state model, is presented.

Basic Model

Assume that figure 2(a) represents a source of engine data having single input $u(t)$ and containing two variables of interest: $x(t)$, which is measurable, and $y(t)$, which is unmeasurable in the actual engine. Let $v(t)$ represent the external conditions of the engine that modify the relations between the engine variables $x(t), y(t)$ and the manipulated variable $u(t)$. Assume that these relations are time-invariant but nonlinear functions of $u(t)$ as well as of $v(t)$, but for constant $v(t) = v_k$ they become linear for small disturbances of $u(t)$.

If $u(t)$ is to be generated by a digital controller, samplers must be incorporated, as shown in figure 2(b). The variables $u(n)$, $x(n)$, and $y(n)$ describe $u(t)$, $x(t)$, and $y(t)$, respectively, only at the sampling instants. Define the system to be at rest at the $n - 1$ sampling instant and $u(n - 1) = u_a$, $x(n - 1) = x_a$, and $y(n - 1) = y_a$. If $u(n) = u_b$ and $u(n + i) = u_a$, where i is any positive integer greater than zero, the system can be defined in terms of a weighting sequence if the resultant approximate impulse (shown in fig. 2(c)) of magnitude $u_b - u_a$ is small enough so as to maintain the simulation in the linear region about x_a and y_a. The resultant discrete impulse transfer function (ref. 4)

$$y(n) - y_a = \sum_{i=0}^{\infty} g_i(u_a, v_a)\left[u(n - i) - u_a\right] \tag{1}$$

completely describes $y(t)$ around u_a and v_a at the sampling instants. The weighting factors $g_i(u_a, v_a)$ are determined from the sampled impulse response and given by the determination equation

$$g_i(u_a, v_a) = \frac{y(n + i) - y_a}{u_b - u_a} \qquad \text{where } i = 1 \rightarrow \infty \tag{2}$$

To evaluate the steady-state accuracy of the model given by equation (1), let $u(n)$ be adjusted so that $u(n - i) = u_c$ for all i values. The variable $y(n)$ will achieve steady state at

$$y(n) = y_a + \sum_{i=0}^{\infty} g_i(u_a, v_a)(u_c - u_a) \tag{3}$$

Note that the accuracy of this steady-state model depends upon the accuracy with which the values of g_i have been determined.

The accuracy of the weighting factors is primarily a function of three considerations:

(1) Inherent accuracy of the data source

(2) Measurement accuracy

(3) Adherence to the linear region of the model

If the data source is a simulation, errors will arise as a result of the inability to accurately define effective areas, volumes, and friction. If the data source is an engine, subtle differences in the fabrications of similar engines could cause weighting factor error.

Measurement accuracy problems are not easily avoided. The impulse disturbance of an engine transmits little power to the data source and could easily lead to signal-to-noise ratios that would significantly affect the g_i accuracy. The primary consideration affecting g_i accuracy, however, is the necessity of strict adherence to the linear region in model applications. Should u_c be such that the operating-point moves outside this region, the g_i may become extremely inaccurate and may result in gross errors in both the dynamic and steady states.

Steady-state nonlinearities can be easily handled by generating appropriate functional relations among the various engine variables. These relations are usually available from the engine design program and are easily refined on actual engines by using steady-state sensors, which are generally available. For these reasons it is not prudent to tie steady-state accuracy to dynamically obtained weighting factors.

To isolate steady-state accuracy from dynamic accuracy, it is necessary that in the steady state the model reduce to

$$y(n) = f_y\left[u(n), x(n), v(n)\right] \tag{4}$$

where the right side of this equation represents an accurate steady-state model of the engine. This is easily accomplished by changing the data source configuration given in figure 2(b) to that given in figure 2(d). In this figure, the dummy variables u' and y' are defined as

$$u'(n) = u(n) - u(n-1) \tag{5}$$

$$y'(n) = y(n) - f_y\left[u(n), x(n), v(n)\right] \tag{6}$$

If an impulse is applied at $u'(n)$, just as described for the development of the weighting factors of equation (2), a set of weighting factors r_i may be determined from

$$r_i(u_a, v_a) = \frac{y'(n+i) - y'_a}{u_b - u_a} \tag{7}$$

These weighting factors then define the following discrete impulse transfer function:

$$y'(n) - y'_a = \sum_{i=0}^{\infty} r_i(u_a, v_a)\left[u'(n-1) - u'_a\right] \tag{8}$$

By definition, y'_a and u'_a are zero because they represent steady-state values. As a result of substituting equations (5) and (6) into equations (7) and (8) and generalizing to any operating point specified by u_j and v_k, the determination equation and the model equation become

$$r_i(u_j, v_k) = \frac{y(n+i) - f_y\left[u(n+i), x(n+i), v_k\right]}{u_b - u_j} \tag{9}$$

$$y(n) = f_y\left[u(n), x(n), v(n)\right] + \sum_{i=0}^{\infty} r_i(u_j, v_k)\left[u(n-i) - u(n-i-1)\right] \tag{10}$$

In steady state, $u(n+i) - u(n+i-1) = 0$, and consequently the model of equation (10) reduces to that specified by equation (4). This effectively isolates steady-state accuracy from the weighting factors and consequently from dynamic accuracy. Note that in the development of the weighting factors of equation (9), the impulse is applied to $u'(n)$. The actual disturbance of the manipulated variable is, therefore, a step function.

Practical Considerations

The model given in equation (10) is not practical. To build this model, the infinite summation must be made finite. This is possible if the engine does not contain a free integrator (i.e., $y(n)$ eventually reaches steady state for constant $u(n)$). This has already been implicitly assumed in the discussion of steady-state relations. Equation (10) can then be rewritten as

$$y(n) = f_y\left[u(n), x(n), v(n)\right] + \sum_{i=0}^{m} r_i(u_j, v_k)\left[u(n-i) - u(n-i-1)\right] \tag{11}$$

where m is determined by the resolution of the digital controller to be that interval at which $r_i(u_j, v_k) \approx 0$ for all $i > m$.

The amount of information necessary to implement equation (11) depends on the engine dynamics and nonlinearities and on the desired accuracy of the $y(n)$ estimate. Steady-state accuracy is assured if f_y can be defined over the operational envelope of the engine (for all $v(t)$) and can be contained within the storage capability of the control. Dynamic accuracy is not only a function of the storage capability of the control but also a function of its calculation-time capability. The calculation time of the estimate is essentially proportional to m. The time may be reduced by extending the control update interval, thereby reducing m. Extension of the update interval also allows for longer calculation times but increases the amount of undesirable digital dynamics inserted by the control into the closed-loop system.

Since dynamic simulation precision may be questionable, the weighting factor method of dynamic identification (or any dynamic identification method based on a simulation) is also questionable. It has been indicated that slight inaccuracies in the determination of the steady-state relations could also compromise the dynamic accuracy of equation (11). Dynamic accuracy may be further compromised because of the dynamic nonlinearity of the engine and the inability to completely define the weighting factors for all possible values of $v(t)$. Even if adequate definition were possible, storage requirements of the weighting factors could be prohibitive.

To alleviate these problems, the next step in the model formulation is the incorporation of a trim function for the model dynamics. Since the steady-state and dynamic terms of equation (11) are essentially distinct, the dynamic trim is easily incorporated without affecting steady-state accuracy, as follows:

$$y(n) = f_y\left[u(n), x(n), v(n)\right] + T_r\left[x(n), v(n)\right] \sum_{i=0}^{m} r_i(u_j, v_k)\left[u(n-i) - u(n-i-1)\right] \tag{12}$$

where T_r is the trim function. The arguments of T_r, $x(n)$, and $v(n)$ imply that it could vary as a function of the engine operating point. Investigation of this function was made empirically and is discussed in a subsequent section of this report.

TF30-P-3 ESTIMATOR MODELS

By using equation (12), models were formulated for estimating the TF30-P-3 engine variables given in table II. Turbine-inlet temperature T_4 and LPC rotor speed N_L were corrected to fan-face conditions (station 2 in fig. 1). The airflows $W_{A,L}$ and $W_{A,H}$ were corrected to their respective compressor-face conditions (stations 2.1 and 2.2, respectively). To form a model using equation (12), three elements are necessary:

(1) Steady-state model

(2) Dynamic weighting factors

(3) Trim function

In discussing the assumptions and simplifications used in generating each element, no attempt is made to optimize the model accuracy by varying the element complexity. A very basic approach is taken in the generation of each element in order to obtain a worst-case evaluation of the modeling technique.

Steady-State Model Generation

It is apparent from equation (9) that the weighting factors and consequently the dynamic accuracy of the model depend heavily on the argument of the steady-state model. The argument that will provide the most accurate dynamic model will be that which minimizes the absolute magnitude of the weighting factors in the dynamic term of the model. This follows from the assumption that the dynamic accuracy of the model is more questionable then the steady-state accuracy. For this reason, three steady-state models were considered, each with arguments of significantly different dynamic content. These arguments (CW_f, $CP_{s,2.2}$, and T_g) are given in table III and were corrected to the fan-face conditions (station 2 in fig. 1). Gage temperature T_g is defined as

$$T_g = \frac{1}{1 + 0.05s}(T_3 - T_2 + T_6) \tag{13}$$

Manufacturer's data indicate a good dynamic correlation between T_g and T_4.

The steady-state functions f_y were derived from the hybrid engine simulation by techniques described in reference 5. A slow ramp in CW_f was inserted into the simulation while the exhaust nozzle was held at minimum area (its normal position during subaugmentation operation). The minimum and maximum CW_f settings were determined by the simulation's range of operation at the two flight conditions necessary for choked and unchoked nozzle operation. The flight conditions used were

(1) Sea-level static (unchoked nozzle operation)

(2) Mach number, M, 1.2; altitude, H, 12 192 meters (choked nozzle operation)

The minimum and maximum CW_f were 0.113 and 0.997 kilogram per second, respectively. At each flight condition a ramp of 100-second duration was used to ensure steady-state engine operation.

The sampled values of the measurable and unmeasurable engine variables were stored in tables of 55 words each at 0.0227-kilogram-per-second increments of CW_f. Each table required nine words of heading. Tables for each variable were formed for three bleed conditions (closed, twelfth-stage open, and seventh-stage open) and at the two flight conditions. The storage requirement for the steady-state functional relation of each variable was $3 \times 2 \times 64 = 384$ words.

The resultant function tables provide the steady-state relations of the engine variables (whether measurable, x(n), or unmeasurable, y(n)) to the manipulated variable $CW_f(n)$ at the sample instant n. Note that, if the engine is not in steady state, these relations will provide the values that the engine variables would eventually achieve if CW_f were held at $CW_f(n)$. Assume that f_{xu} and f_{yu} represent the functional relation between x(n) and $CW_f(n)$ and between y(n) and $CW_f(n)$, respectively, and that f_{xu} is a monotonically increasing function. Then the inverse function f_{xu}^{-1} is unique and f_{yx}, the steady-state functional relation between y(n) and x(n), may be determined by using the equation

$$f_{yx}\left[x(n)\right] = f_{yu}\left\{f_{xu}^{-1}\left[x(n)\right]\right\} \tag{14}$$

The steady-state functional relations between each variable and CW_f are given in figure 3. Only closed compressor bleed conditions are given for the sake of simplicity. The effects of compressor bleed are discussed in reference 5. Note that the curves representing unchoked nozzle operation blend with those representing choked nozzle operation at high values of CW_f. This is due to the nozzle choking at high rotor speeds even at sea-level-static conditions. Also note that the final discrete model does not depend on this method of steady-state modeling. Any desirable method of steady-state modeling may be used.

Weighting Factor Generation

The determination equation (eq. (9)) was used to generate the weighting factors for the mathematical models. The $r_i(u_j, v_k)$ were determined for the v_k given in table IV for each u_j given in table V. When the simulation achieved steady state at $CW_f = u_j$, CW_f was stepped to a value of $u_j + 0.113$ kilogram per second. This magnitude was chosen as the minimum to give good measurement resolution. Each y-variable and x-variable was sampled, corrected as indicated previously, and stored. The sample time

was chosen to be 50 milliseconds to allow adequate calculation time for the estimates. According to reference 1, this is the maximum interval that may be used without dynamic degradation. Sixty-four samples were taken of each variable per CW_f disturbance at each condition, allowing for a total transient time of 3.2 seconds.

The sampled data contained sufficient information when coupled with the steady-state functions of figure 3 to solve equation (9) for the weighting factors. Weighting factors could then be developed by using either CW_f or the transient data for $x(n)$ as the argument of the steady-state function relating it to $y(n)$. The result at each sample instant was subtracted from the sampled $y(n)$ at that instant. The $r_i(u_j, v_k)$ were formed at each sample i by dividing the result by the step magnitude.

From equation (9), specific weighting factors for the CW_f input were developed as

$$r_{yw,i}(u_j, v_k) = \frac{y(n+i) - f_{yw}\left[CW_f(n+i)\right]}{0.113} \tag{15}$$

at $v_k = v_1$ and for the u_j in table V. These are given in figure 4 to illustrate the nonlinearities of the weighting factors as a function of setpoint u_j. The range of u_j represents a range in CN_H of 9788 to 14 230 rpm, which is greater than the range in CN_H from idle to intermediate.

Since the argument of the steady-state function used to obtain these weighting factors is CW_f, the weighting factors represent the response of each variable to a step in CW_f at each operating point. The $i = 1$ factor is approximately the gain of this response. This is true since in the first 50 milliseconds the measured $y(n + 1)$ has barely moved, whereas the steady-state model has reached its final value. The time for the response to reach zero is proportional to the time constant; and overshoot, if any, is proportional to system damping. Note that, as j increases, the time to reach steady state decreases. The difference between the final value of the weighting factors and zero (if steady state has been reached) represents inaccuracies in the steady-state model.

It should be pointed out that the step in CW_f occurred at $i = 0$. Since the engine is nonanticipatory, the weighting factor at $i = 0$ is zero.

The effect of HPC bleed on the weighting factors is also illustrated in figure 4. At $u_j = u_1$, the HPC bleed was opened and the $u_j = u_1$ weighting factors were again generated. As compared with the effects of variations of u_j, the bleed effects on the weighting factors are negligible.

Figure 5 compares the effects of setpoint u_j and LPC bleed at the external condition $v_k = v_2$ on weighting factors again generated by using equation (15). The effect of LPC bleed is also negligible. The effects of setpoint, however, are notably different from those at $v_k = v_1$ (fig. 4). The difference is due to exhaust nozzle choking effects. At $v_k = v_1$ (fig. 4) the exhaust nozzle is unchoked for setpoints u_1, u_2, and u_3. At

corresponding setpoints at $v_k = v_1$, the exhaust nozzle is choked. The major difference between the weighting factors of figure 4 and those of figure 5 occurs at these setpoints.

Figure 6 shows weighting factors developed from the determination equation

$$r_{yP,i}(u_j, v_k) = \frac{y(n+i) - f_{yW}\left\{f_{PW}^{-1}\left[CP_{s,2.2}(n+i)\right]\right\}}{0.113} \tag{16}$$

at $v_k = v_1$ and for the u_j in table V. Here the inverse functional relation of equation (14) has been used to relate the unmeasurable variables directly to $CP_{s,2.2}$. Since in this case the argument of the steady-state model is $CP_{s,2.2}$ rather than CW_f as in equation (15), these weighting factors reflect the relative dynamics of the y-variables to $CP_{s,2.2}$ (the closer they are dynamically, the smaller the absolute magnitude of the weighting factors). Note that CN_L and $CW_{A,L}$ are dynamically very close to $CP_{s,2.2}$.

In figure 7, weighting factors were generated by using equation (17). As expected, CT_4 is dynamically very close to CT_g:

$$r_{yT,i}(u_j, v_k) = \frac{y(n+i) - f_{yW}\left\{f_{TW}^{-1}\left[T_g(n+i)\right]\right\}}{0.113}$$

Storage and timing requirements for the dynamic model depend upon the number of sets of weighting factors needed for each variable and also upon the number of weighting factors contained in each set. For the weighting factors shown in figures 4 and 5, 64 words of data storage are necessary per condition per variable. The computation of the dynamic model requires a minimum of 64 multiplications and additions and 128 loads and stores. For the digital computer described in table I this amounts to a minimum of 0.561 millisecond of computation time.

Trim Function Generation

Review of figures 4 and 5 makes it apparent that the problems associated with developing weighting factors to exactly define engine dynamics for all possible steps in CW_f at all engine operating points are prohibitive. It would be desirable to be able to incorporate a simple trim function with a single set of weighting factors that would allow adequate definition of engine dynamics under all circumstances. Also, since the dynamics of the computerized engine simulation from which the weighting factors would be

developed are assumed to contain some degree of inaccuracy, a trim function may be necessary in applying the estimator models to actual engine control systems.

Instead of a detailed analysis to determine an optimum trim function for each variable, an experimental generation of a simple trim function was performed. The trim function obtained by using this method provided a worst-case evaluation of the discrete estimator model. A more detailed analysis in the generation of the trim function could only improve the accuracy of the estimator model.

The first step in the experimental development of a trim function was to choose a single set of weighting factors for use in the estimator model. The weighting factors corresponding to choked nozzle operation were chosen since under the majority of circumstances the engine is operating under this condition. The weighting factors obtained at lowest CN_H are seen from figures 5 to 7 to contain the greatest dynamic content. The weighting factors for use in the estimator models, therefore, were chosen to be those represented by the solid lines of figures 5 to 7.

The second step in the development was to choose the argument of the trim function. The purpose of the trim function is to modify the weighting factors to account for the variation in engine dynamics from that encountered at the point at which the weighting factors were obtained. A large contribution to the dynamic variation can be related to the mechanical speed of the rotors (fig. 4). For this reason the dynamic trim was made a function of mechanical speed. For simplicity, a straight-line function was chosen, the intercept and slope of which were empirically derived.

The trim function $T_r(N_H)$ was developed experimentally for the estimation of $CW_{A,L}$ at $v_k = v_2$. The estimator model for $CW_{A,L}$ was chosen as

$$CW_{A,L} = f_{WLW}(CW_f) + T_r(N_H) \sum_{i=1}^{64} r_{WLW,i}(u_1, v_2)\left[CW_f(n - i) - CW_f(n - i - 1)\right] \qquad (18)$$

This was done by observing the error between the measured value of $CW_{A,L}$ and its estimated value for a 4-second ramp in CW_f from 0.113 kilogram per second to 0.793 kilogram per second. A straight-line function was chosen, and its intercept and slope were varied until a minimum error response for the ramp was observed. The resultant function was

$$T_r(N_H) = -1.25\times10^{-4}\, N_H + 1.875 \qquad (19)$$

The use of N_H in the model dictates that it must be measurable.

The solid line in figure 8 is a plot of the trim function. The optimum trim function should have some relation to the area contained in the weighting factor curves of figure 5, relative to the weighting factors obtained at u_1 and v_2 for each variable. As an

attempt to verify this, a relative dynamic power content (RDPC) was formed as

$$RDPC_j = \left[\frac{\sum_{i=1}^{64} r^2_{yW,i}(u_j, v_2)}{\sum_{i=1}^{64} r^2_{yW,i}(u_1, v_2)} \right]^{1/2} \tag{20}$$

The RDPC's for selected variables are shown in figure 8 for comparison with the empirically derived trim function.

Note that the RDPC's are closer to the trim function at high values of N_H. This seems to indicate that matching of dynamics is more significant at high rotor speeds than at low speeds. Note also that the RDPC's of $CW_{A,L}$ fall very close to the line, suggesting a definite correlation between the relative dynamic power and the optimum trim function. No attempt was made to further optimize the trim function or to find a better correlation with the optimum. Further work in this area could only improve the results presented herein, and these are considered sufficient to evaluate the concept of discrete modeling.

EVALUATION OF ESTIMATOR MODELS

Three estimator models were evaluated in this study. These were

$$y(n) = f_{yW}(CW_f) + T_r(N_H) \sum_{i=1}^{64} r_{yW,i}(u_1, v_2)\left[CW_f(n-i) - CW_f(n-i-1)\right] \tag{21}$$

$$y(n) = f_{yW}\left[f^{-1}_{PW}(CP_{s,2.2})\right] + T_r(N_H) \sum_{i=1}^{64} r_{yP,i}(u_1, v_2)\left[CW_f(n-i) - CW_f(n-i-1)\right] \tag{22}$$

$$y(n) = f_{yW}\left[f^{-1}_{TW}(CT_g)\right] + T_r(N_H) \sum_{i=1}^{64} r_{yT,i}(u_1, v_2)\left[CW_f(n-i) - CW_f(n-i-1)\right] \tag{23}$$

where the $y(n)$ are given in table II, the $r_{yW,i}$ are given in figure 5 ($u_j = u_1$, bleed closed), the $r_{yP,i}$ are given in figure 6 ($u_j = u_1$), and the $r_{yT,i}$ are given in figure 7 ($u_j = u_1$). The steady-state functions are given in figure 3.

The estimates developed from equation (21) for the variables given in table II by using the trim function described in equation (19) are compared with those estimates obtained by using a unity trim function $T_r(N_H) = 1$ in figure 9. The transients shown in

figure 9 and in figures 11 to 13 represent the difference between the actual measurement of the variable on the hybrid simulation and its estimated value over a typical engine transient. The results are shown at the external operating conditions of table IV.

The engine transient used in generating these data was a throttle step from idle to full augmentation with the engine simulation operating under its bill-of-material control (ref. 1). The transients used to obtain the data of figures 9 and 11 to 13 are given in figure 10 in terms of fuel flow rate W_f for each of the v_k in table IV.

The value of the trim function is apparent in figure 9 by comparing the solid line (trim defined by eq. (19)) to the dashed line (unity trim). At nozzle choked conditions (v_2,v_3, and v_4), estimation errors are generally smaller than those occurring at an unchoked nozzle condition (v_1). This may be due in part to the trim function being developed at v_2 but is due mostly to the weighting factors used in the model for dynamic estimation at condition v_1 also being obtained at v_2. (Note the difference between the weighting factors of fig. 4 and those of fig. 5.)

Improvement in the accuracy of the estimates of figure 9 might be expected with the use of a more complex dynamic model. However, improvement could also be obtained with a model of equivalent complexity if the argument of the steady-state model were made more dynamically accurate. The more dynamically accurate this argument becomes, the smaller the weighting and consequently the smaller the effects of operating condition on variable dynamics.

Figure 11 compares the estimates developed from equation (22), which uses $CP_{s,2.2}$ as the argument of the steady-state term, for v_1 to v_4. And figure 12 compares the estimates developed from equation (23), which uses CT_g as the argument of the steady-state term, for v_1 to v_4. Figure 11 shows definite improvement in estimation accuracy over figure 9 for all variables, with the exception of CT_4 and possibly $CW_{A,H}$. This indicates a closer dynamic correspondence of $CW_{A,L}$ and CN_L with $CP_{s,2.2}$ than between these variables and CW_f.

Figure 12 indicates a strong dynamic correlation between CT_4 and CT_g. This follows from the large reduction in CT_4 estimation error over that resulting from the models of equations (21) and (22). Note that the final error in each transient of this figure is significantly larger than the final error in the transients shown in figures 9 and 11. This implies inaccuracies in the steady-state model relating CT_g to CW_f.

Airflow and combustor temperature are perhaps the two most unmeasurable variables in any engine. The preceding discussion suggests that $CP_{s,2.2}$ and CT_g could possibly be used without dynamic compensation as substitutes for $CW_{A,H}$ and CT_4, respectively. To evaluate this possibility, the following estimator models were formed:

$$CW_{A,H} = f_{WHW}\left[f_{PW}^{-1}(CP_{s,2.2})\right] \tag{24}$$

$$CT_4 = f_{T4W}\left[f_{TW}^{-1}(CT_g)\right] \tag{25}$$

which relate high compressor corrected airflow and corrected combustor temperature to $CP_{s,2.2}$ and CT_g, respectively, through the appropriate steady-state relations. The results are presented in figure 13. Although the estimation errors are somewhat larger than those obtained with dynamic compensation, these estimates could still prove useful in some applications.

CONCLUSIONS

The method of discrete modeling described in this report provides not only a straightforward means of generating estimates of unobservable variables, but also provides the control engineer with a useful means of evaluating relations between engine variables. The method is easily automated. It is tailored for formulation and implementation on a digital computer, allowing for easy adaptation into a digital control system.

Isolating the steady-state model from the dynamic model permits the original steady-state design equations, or any simplification of these equations, to be included into the model without consideration of whether the dynamics to be included affect steady-state accuracy. Dynamic model accuracy on the other hand may be enhanced though the proper choice of the argument of the steady-state function. The closer dynamically the observed argument is to the variable to be estimated, the smaller the dependence of the model on the weighting factors and consequently the higher the model accuracy.

Applying the modeling method to the estimation of TF30-P-3 engine variables reveals that compressor bleeds have little effect upon dynamic accuracy as compared with the effects of engine setpoint and degree of exhaust nozzle choking. The effects of engine setpoint changes may be somewhat accounted for by applying a straight-line function of high-pressure-compressor (HPC) rotor speed as a trim of a dynamic mode developed at a single setpoint.

Finally, it may be concluded that, with a proper steady-state relation, gage temperature (as described herein) and low-pressure-compressor (LPC) discharge static pressure may be used as alternate measurements for turbine-inlet temperature and HPC corrected airflow, respectively.

Lewis Research Center,
National Aeronautics and Space Administration,
Cleveland, Ohio, June 14, 1976,
505-05.

APPENDIX - SYMBOLS

CN	corrected rotor speed, rpm
CP	corrected pressure, kg/m^2
CT	corrected temperature, K
CW	corrected flow rate, kg/sec
CW_f	corrected fuel flow rate, kg/sec
f	functional relation
g	generalized weighting factor
H	altitude, m
i	sample indexing variable (integer)
M	Mach number
N	rotor speed, rpm
n	integer
P	pressure, kg/m^2
RDPC	relative dynamic power content
r	dynamic weighting factor
s	Laplace operator, sec^{-1}
T	temperature, K
T_r	trim function
t	time, sec
u	generalized manipulated variable
u_j	generalized internal engine operating condition
v_k	generalized external engine operating condition
W	flow rate, kg/sec
W_f	fuel flow rate, kg/sec
x	generalized observable variable
y	generalized unobservable variable
z	z-transform operator

Subscripts:

A	air
a, b, c	particular values
e	estimate
g	gage
H	high-pressure compressor
i	sample indexing variable
L	low-pressure compressor
m	measured
PW	functional designation relating $CP_{s,2.2}$ to CW_f
s	static
ss	steady state
TW	functional designation relating CT_g to CW_f
T4W	functional designation relating CT_4 to CW_f
WHW	functional designation relating $CW_{A,H}$ to CW_f
WLW	functional designation relating $CW_{A,L}$ to CW_f
WNW	functional designation relating CN_L to CW_f
xu	functional designation relating x to u
yP	functional designation relating y to CP
yT	functional designation relating y to CT
yu	functional designation relating y to u
yW	functional designation relating y to CW_f
yx	functional designation relating y to x
1, 2, 2.1, 2.2, 3, 4, 4.1, 5, 6	engine station numbers as defined in fig. 1

Superscript:

'	difference variable

REFERENCES

1. Cwynar, David S.; and Batterton, Peter G.: Digital Implementation of the TF30-P-3 Turbofan Engine Control. NASA TM X-3105, 1975.

2. Szuch, John R.; and Bruton, William M.: Real-Time Simulation of the TF30-P-3 Turbofan Engine Using a Hybrid Computer. NASA TM X-3106, 1974.

3. Arpasi, Dale J.; Zeller, John R.; and Batterton, Peter G.: A General-Purpose Digital System for On-Line Control of Airbreathing Propulsion Systems. NASA TM X-2168, 1971.

4. Kuo, Benjamin C.: Analysis and Synthesis of Sampled-Data Control Systems. Prentice Hall, Inc., 1963, p. 74.

5. Hrach, Frank J.; Arpasi, Dale J.; and Bruton, William M.: Design and Evaluation of a Sensor Fail-Operational Control System for a Digitally Controlled Turbofan Engine. NASA TM X-3260, 1975.

TABLE I. - DIGITAL SYSTEM CAPABILITIES

Digital computer	
Magnetic core memory size, words	16 384
Word length, bits plus parity	16
Memory cycle time, nsec	750
Add time, μsec	1.5
Subtract time, μsec	1.5
Multiply time, μsec	4.5
Divide time, μsec	8.25
Load time, μsec	1.5
Store time, μsec	1.5
Indirect addressing	Infinite
Indexing	Total memory
Priority interrupts	28 Separate levels
Index registers:	
Independent	1
In conjunction with lower accumulator	1
Physical size, cm (in.):	
Width	60.1 (24)
Height	157.5 (62)
Depth	76.2 (30)
Interval timers	
Complement	2
Accuracy, clock pulses	±1
Clock rates, kHz	572, 286, 160, 143, 80, 71.5, 40, 35.75, 20, 10
Counter	16-Bit binary
Output	Priority interrupt to computer
Analog acquisition unit	
Number of multiplexers, digitizers, samples, and holds	2
Overall sample rate (maximum), kHz	40
Resolution of digital data, bits	12 (plus sign)
Output code	Two's complement
Number of channels	64
Input range, V full scale	±10
Input impedance, MΩ (shunted by 10 pF)	10
Maximum source resistance, Ω	1000
Conversion time, μsec	38
Input setting time, μsec	9
Sample-and-hold aperture time, nsec	500
Safe input voltages, V	±20 sustained ±100 for less than 100 μsec
Total error with calibration, percent	0.073

TABLE I. - Concluded. DIGITAL SYSTEM CAPABILITIES

Frequency acquisition unit	
Number of channels	10
Nature of input	Continuously varying or pulsatile
Resolution of digital data, bits	12
Switch selectable clock rates, kHz	20, 80, 100, 400, external
Overall accuracy, bits	±1
Undate rate	Once per cycle of input frequency
Maximum input frequency, kHz	1
Input amplitude range	100 mV to 30 V peak to peak
Analog output unit	
Total number of digital-to-analog conversion channels	26
Resolution (10 channels), bits	12 (plus sign)
Resolution (16 channels), bits	11 (plus sign)
Output voltage range, V full scale	±10
Output current (maximum), mA	10
Output impedance, Ω	<1
Accuracy (12 bit), percent of full scale	±0.1
Accuracy (13 bit), percent of full scale	±0.05
Slew rate, V/μsec	1
Settling time for 10-V step to within 0.05 percent of final value, μsec	20
Logical output unit	
Number of electronic switch outputs	32
Number of contact closure outputs	32
Maximum voltage, V	30
Maximum current, mA	100
Priority interrupt processor	
Number of channels	10
Input impedance, kΩ	47
Input voltage range, V	±10
Comparator switching	Trigger on rise or fall
Comparator hysteresis	Adjustable from 35 mV to 650 mV
Comparator output, V	+7
Monostable multivibrator:	
Pulse width, μsec	3
Pulse height, V	+7

TABLE II. - DESCRIPTION OF ENGINE VARIABLES

TO BE ESTIMATED

Estimated variable	Description
CN_L	Corrected low-pressure-compressor rotor speed, $N_L/\sqrt{\theta_2}$
$CW_{A,L}$	Corrected low-pressure-compressor airflow, $W_{A,2.2}(\delta_{2.1})/\sqrt{\theta_{2.1}}$
$CW_{A,H}$	Corrected high-pressure-compressor airflow, $W_{A,3}(\delta_{2.2})/\sqrt{\theta_{2.2}}$
CT_4	Corrected turbine-inlet temperature, T_4/θ_2

TABLE III. - DESCRIPTION OF ARGUMENTS TO BE

USED IN THE GENERATION OF ESTIMATES

Argument variable	Description
CW_f	Corrected main-combustor fuel flow, $W_f/(\delta_2)(\sqrt{\theta_2})$
$CP_{s,2.2}$	Corrected low-pressure-compressor discharge static pressure, $P_{s,2.2}/\delta_2$
CT_g	Corrected gage temperature, T_g/θ_2

TABLE IV. - EXTERNAL ENGINE TEST CONDITIONS

Generalized external engine operating condition, v_k, where k =	Engine external conditions	
	Mach number, M	Altitude, H, m
1	0	0 (sea-level static)
2	1.2	12 192
3	1.2	3 048
4	2.2	15 240

TABLE V. - ENGINE SETPOINTS FOR

WEIGHTING FACTOR

DETERMINATION

Generalized internal engine operating conditions, u_j, where j =	Corrected main-combustor fuel flow (CW_f) setpoint, kg/sec
1	0.113
2	.227
3	.340
4	.453
5	.680

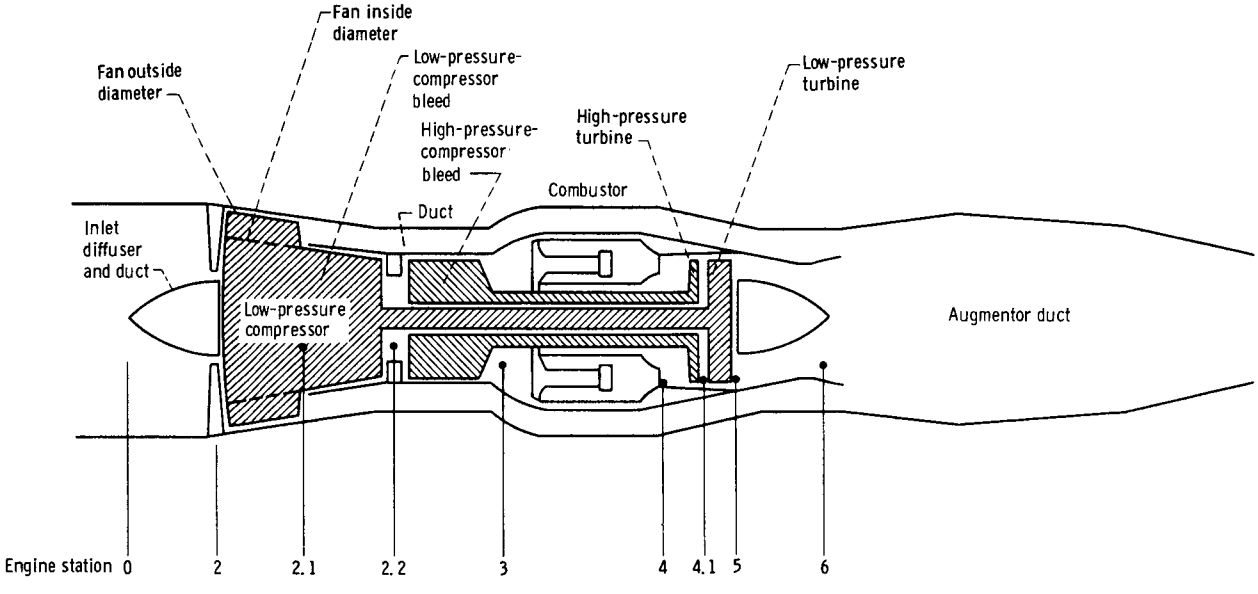

Figure 1. - Schematic representation of TF30-P-3 afterburning turbofan engine with station designations.

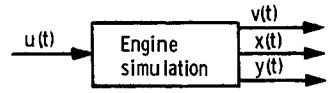

(a) Simplified block diagram of an engine simulation.

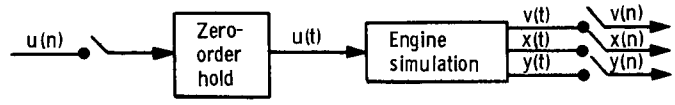

(b) Discretized version of the simplified block diagram.

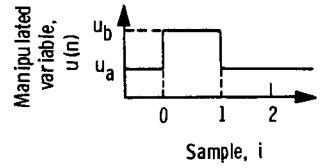

(c) Approximate impulse with duration of 1 sample period.

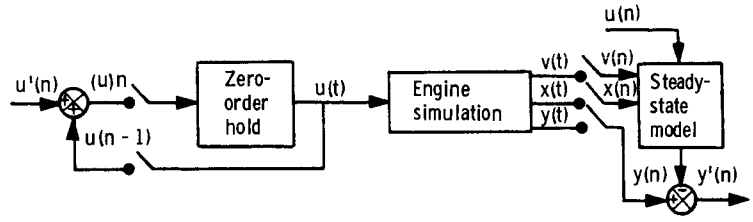

(d) Dynamic model development.

Figure 2. - Mathematical model development.

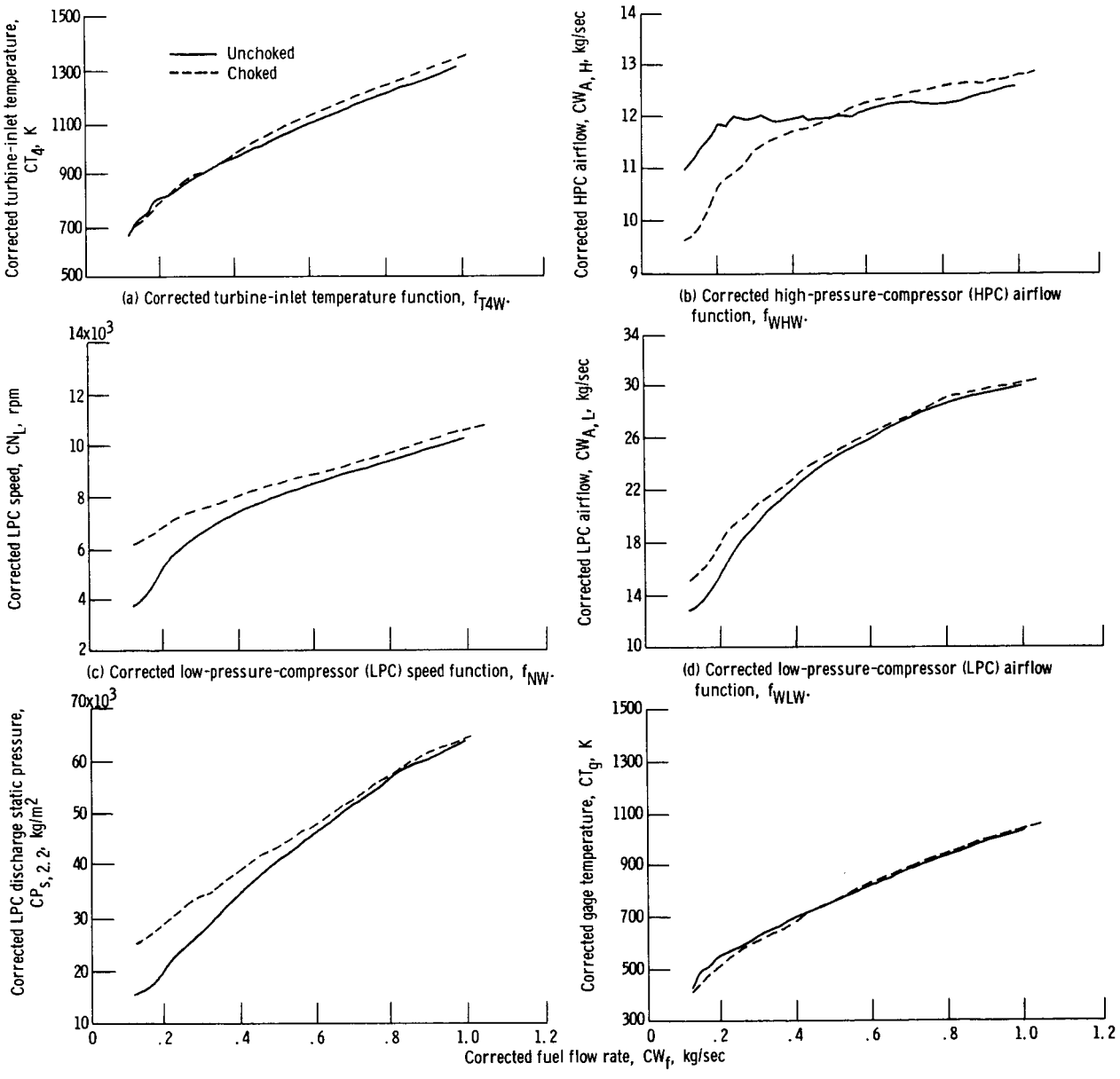

(a) Corrected turbine-inlet temperature function, f_{T4W}.

(b) Corrected high-pressure-compressor (HPC) airflow function, f_{WHW}.

(c) Corrected low-pressure-compressor (LPC) speed function, f_{NW}.

(d) Corrected low-pressure-compressor (LPC) airflow function, f_{WLW}.

(e) Corrected low-pressure-compressor (LPC) discharge static-pressure function, f_{PW}.

(f) Corrected gage temperature function, f_{TW}.

Figure 3. - Steady-state relations for choked and unchoked nozzle conditions.

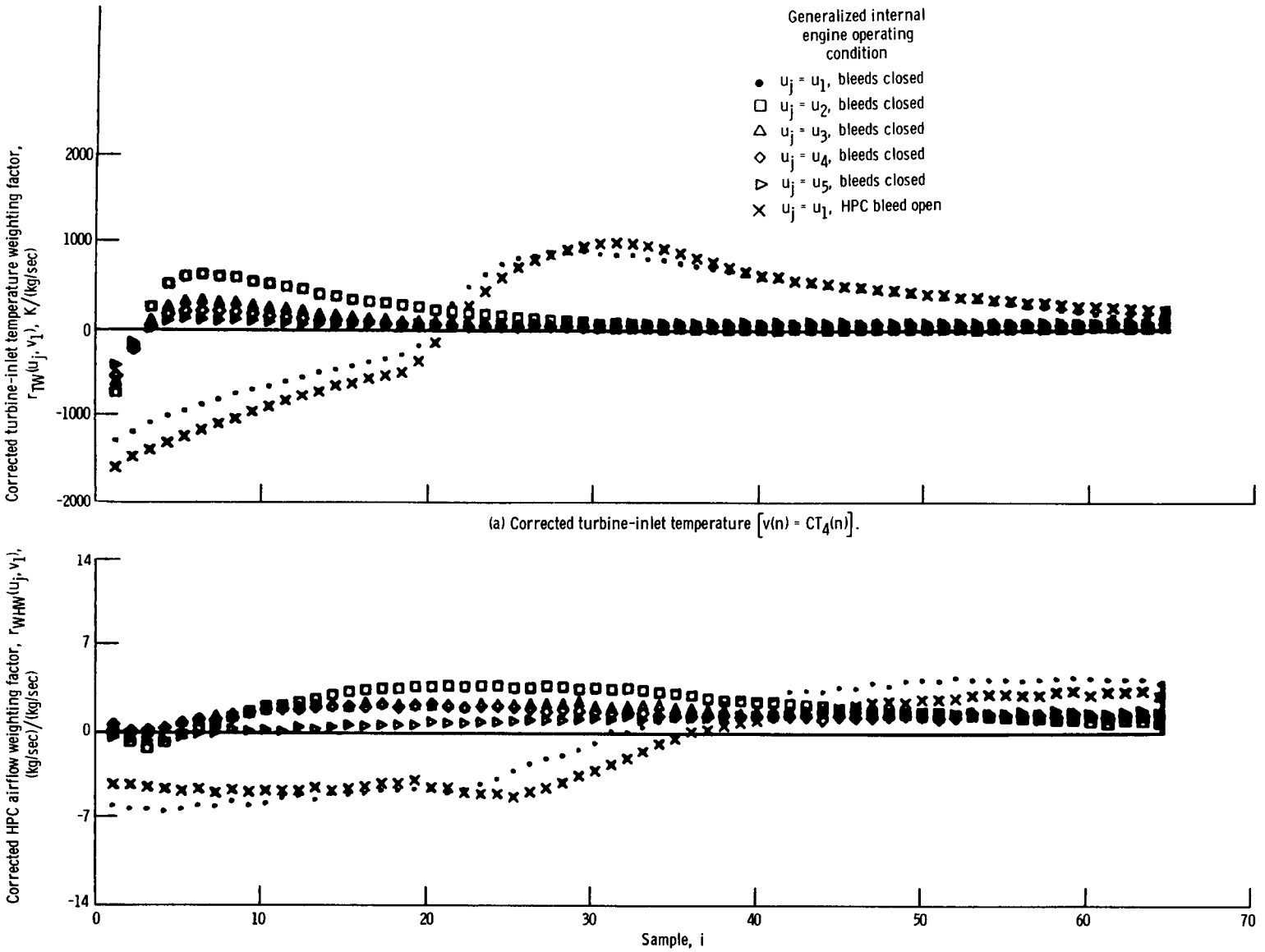

Figure 4. - Effects of corrected-fuel-flow-rate CW_f operating point and high-pressure-compressor bleed on weighting factors derived by using CW_f as the argument of the steady-state model and for a 0.113-kilogram-per-second step in CW_f at the generalized external operating condition $v_k = v_1$.

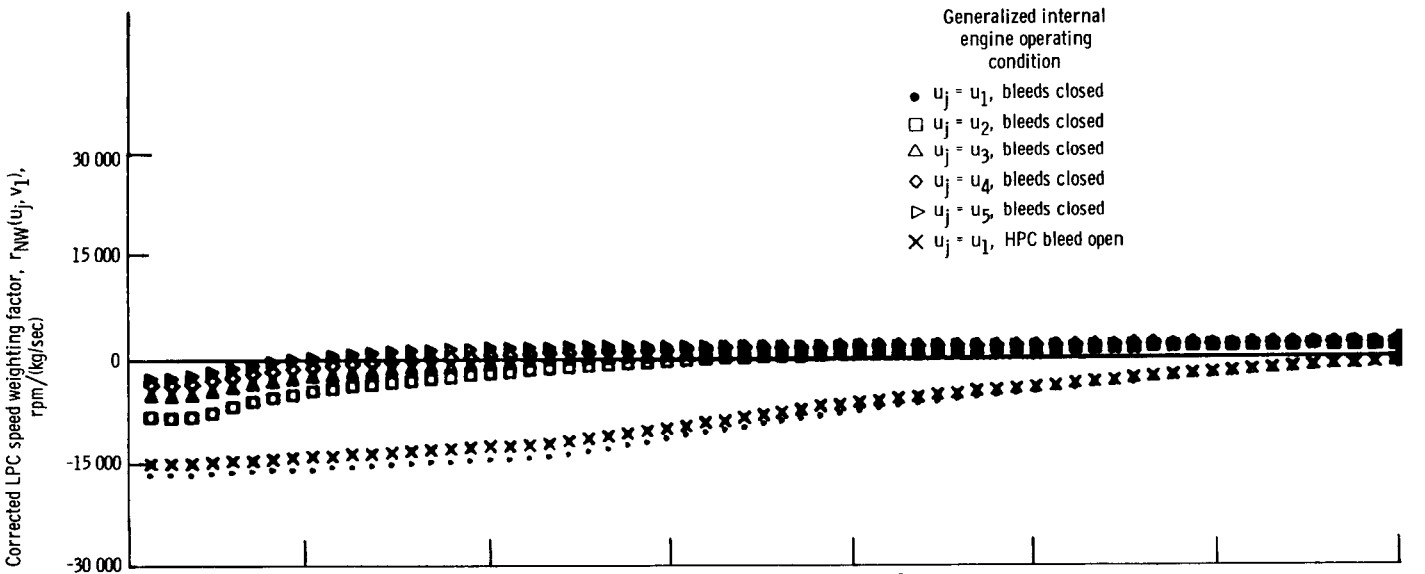

(c) Corrected low-pressure-compressor (LPC) speed $\left[y(n) = CN_L(n)\right]$.

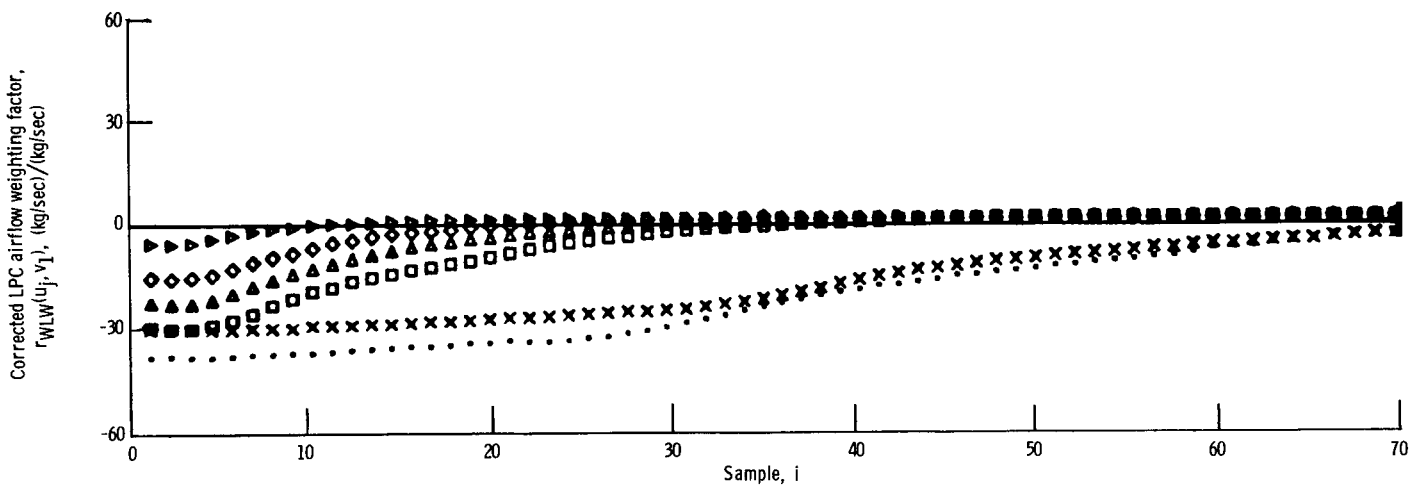

(d) Corrected low-pressure-compressor (LPC) airflow $\left[y(n) = CW_{A,L}(n)\right]$.

Figure 4. - Concluded.

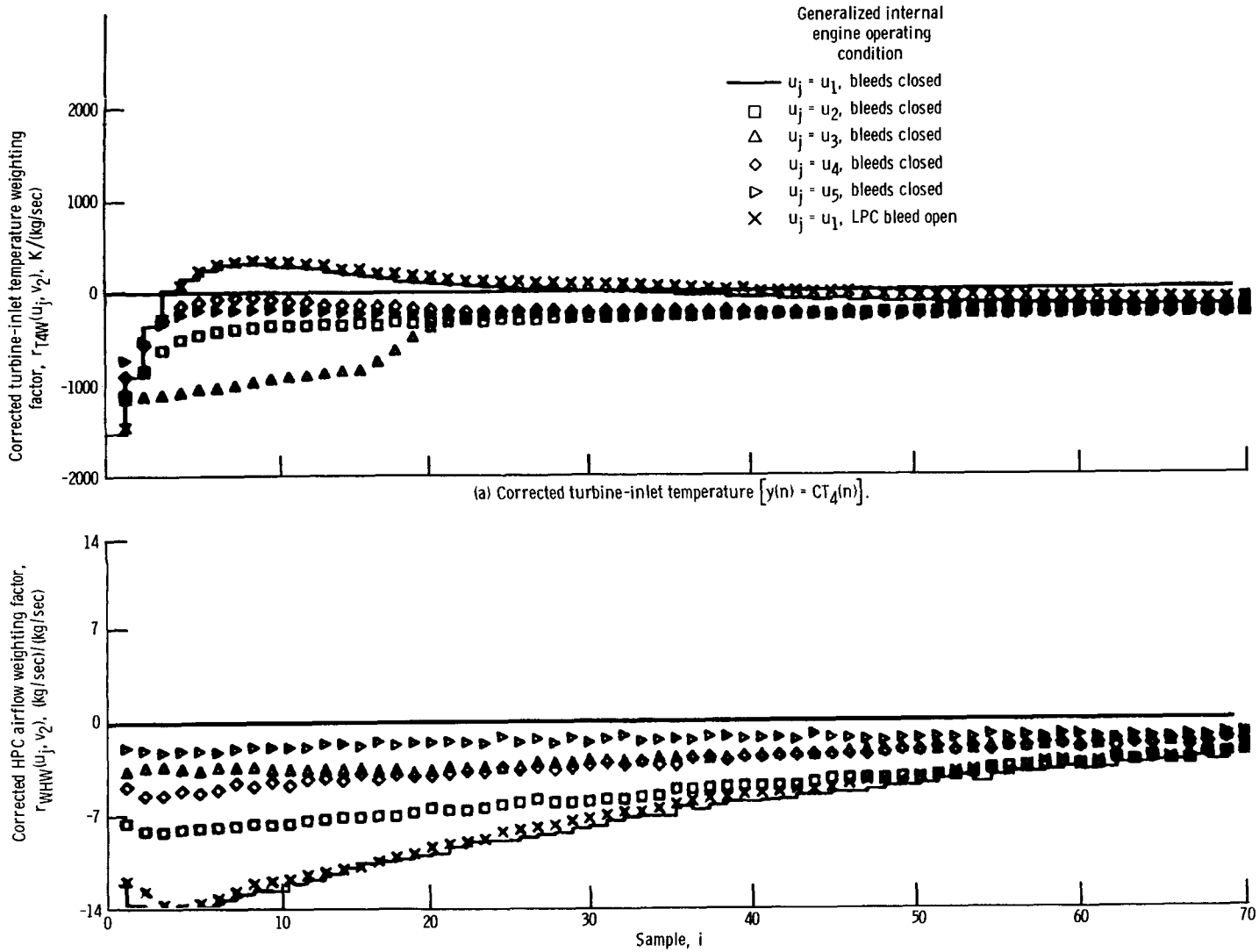

Figure 5. - Effects of corrected-fuel-flow-rate CW_f operating point and low-pressure-compressor bleed on weighting factors derived by using corrected gage temperature CT_g as the argument of the steady-state model and for a 0.113-kilogram-per-second step in CW_f at the generalized external operating condition $v_k = v_2$.

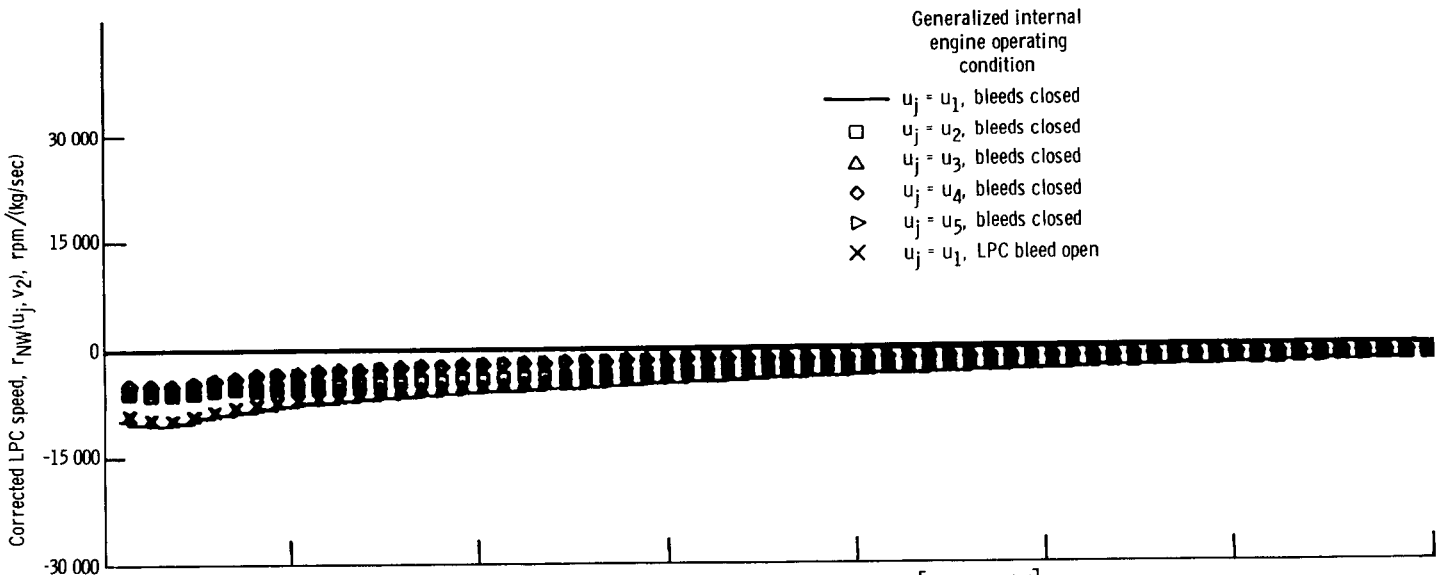

(c) Corrected low-pressure-compressor (LPC) speed $[y(n) = CN_L(n)]$.

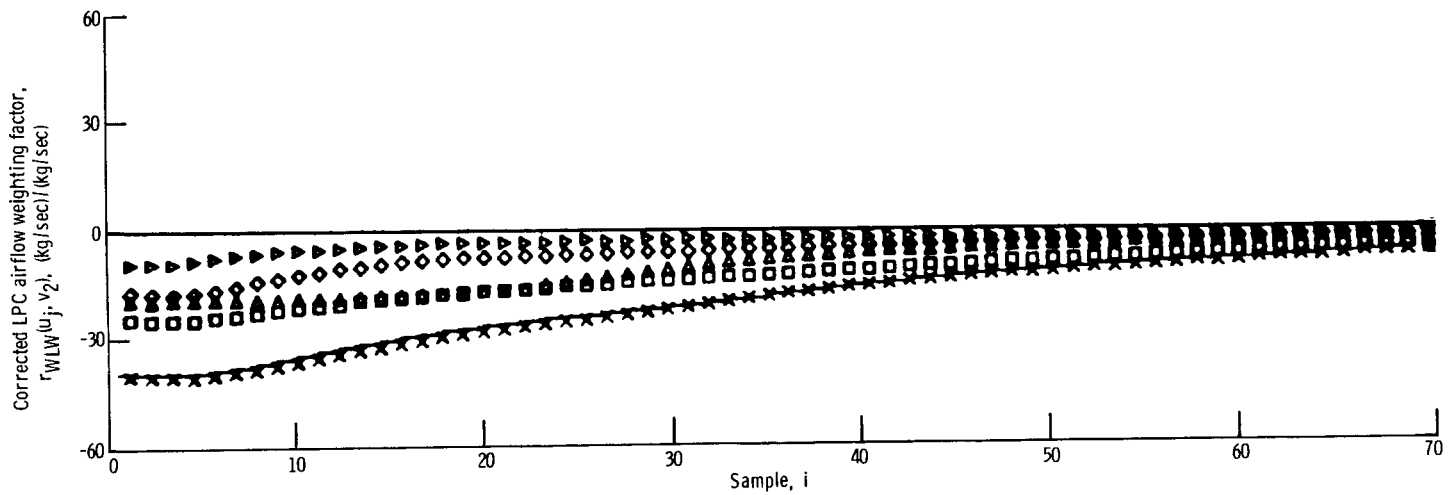

(d) Corrected low-pressure-compressor (LPC) airflow $[y(n) = CW_{A,L}(n)]$.

Figure 5. - Concluded.

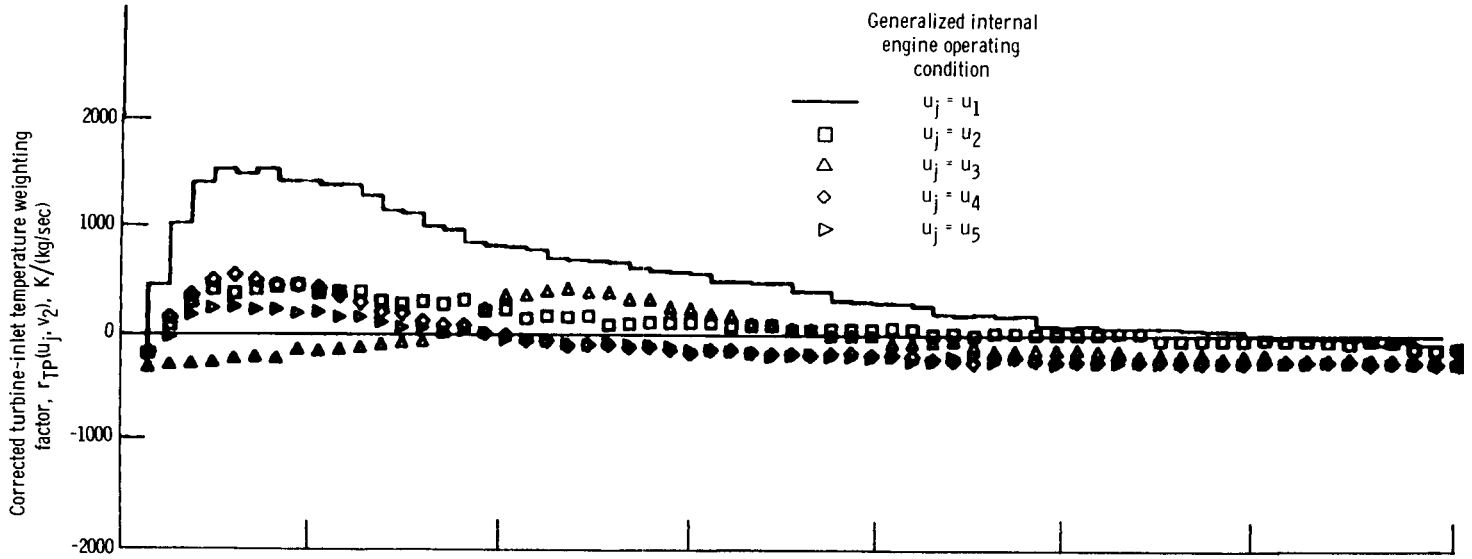

(a) Corrected turbine-inlet temperature $\left[y(n) = CT_4(n)\right]$.

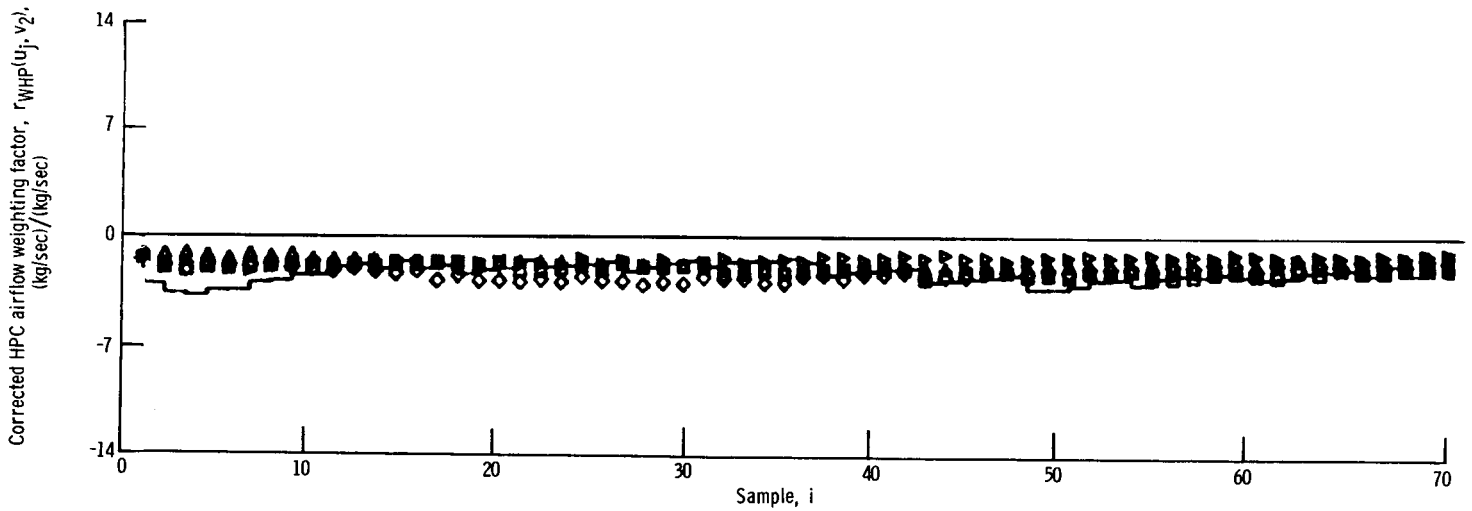

(b) Corrected high-pressure-compressor (HPC) airflow $\left[y(n) = CW_{A,H}(n)\right]$.

Figure 6. - Effects of corrected-fuel-flow-rate CW_f operating point on weighting factors derived by using corrected low-pressure-compressor discharge static pressure $CP_{s,2.2}$ as the argument of the steady-state model and for a 0.113-kilogram-per-second step in CW_f at the generalized external operating condition $v_k = v_2$ with both bleeds closed.

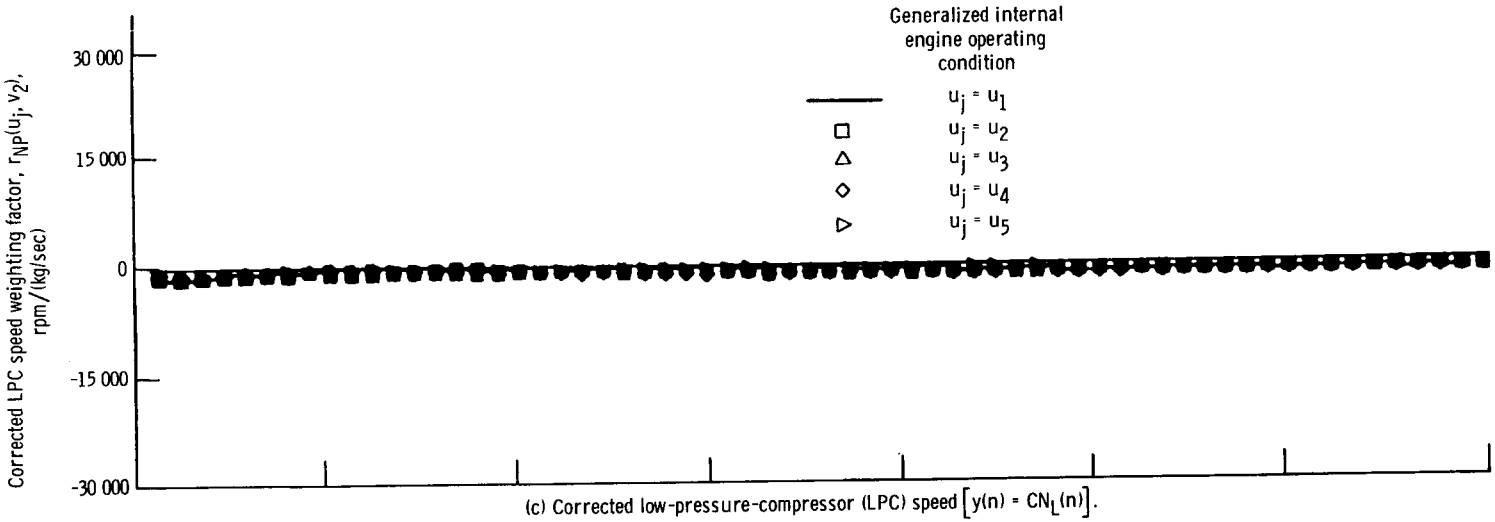

(c) Corrected low-pressure-compressor (LPC) speed $\left[y(n) = CN_L(n)\right]$.

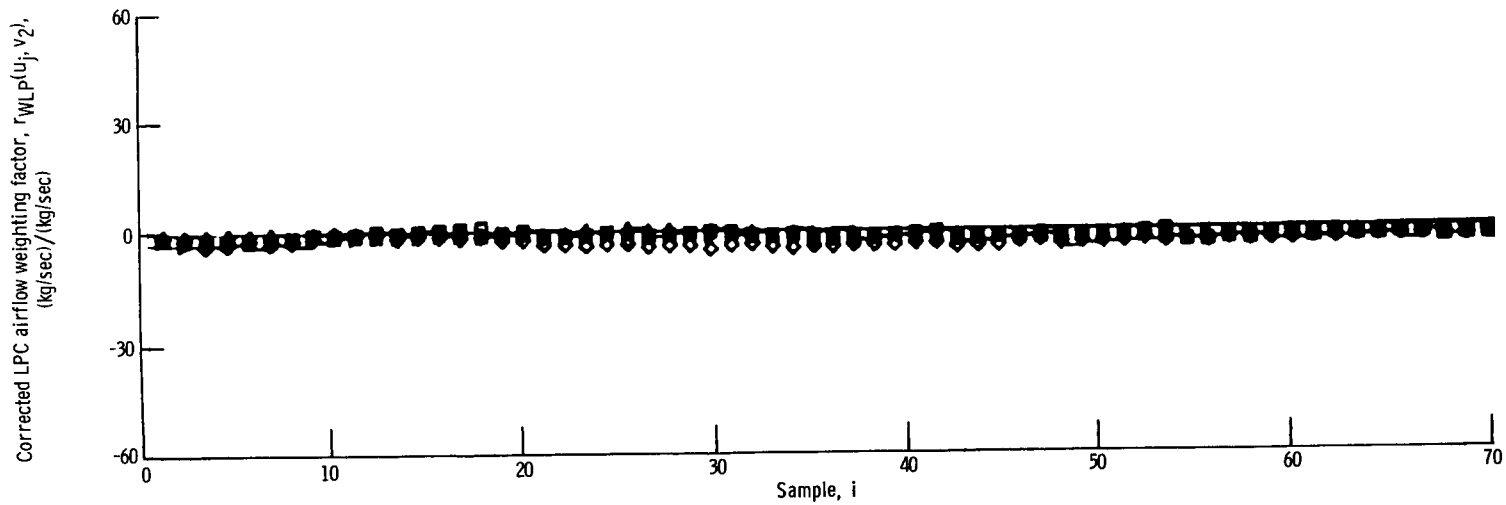

(d) Corrected low-pressure-compressor (LPC) airflow $\left[y(n) = CW_{A,L}(n)\right]$.

Figure 6. - Concluded.

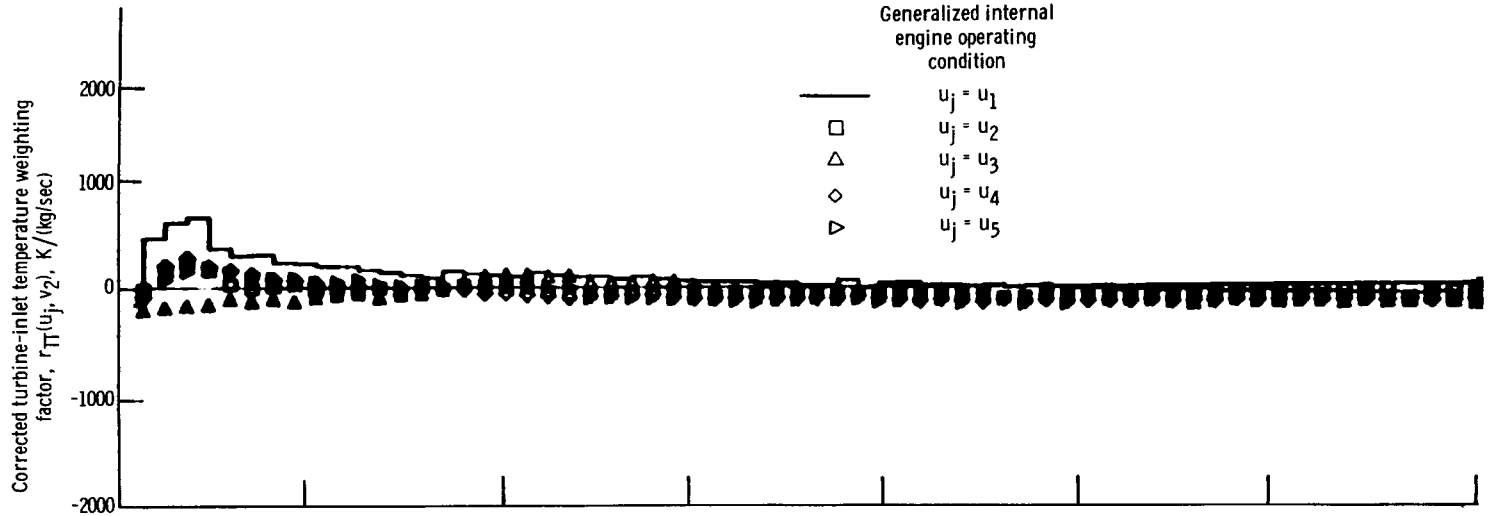

(a) Corrected turbine-inlet temperature $\left[y(n) = CT_4(n)\right]$.

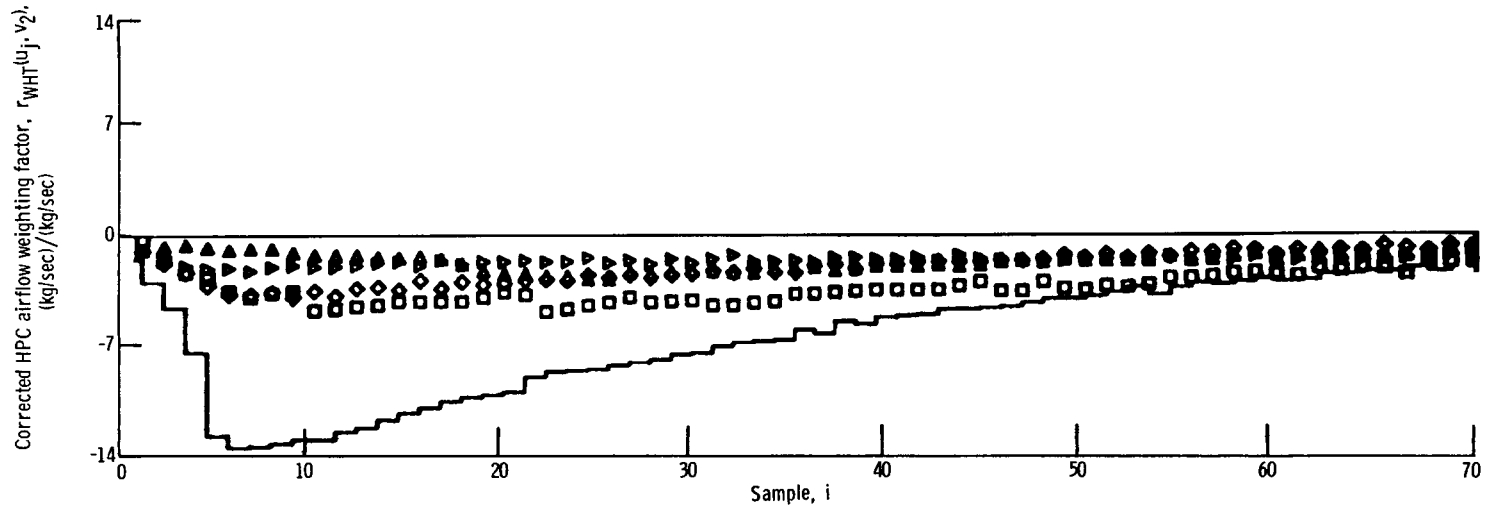

(b) Corrected high-pressure-compressor (HPC) airflow $\left[y(n) = CW_{A,H}(n)\right]$.

Figure 7. - Effects of corrected-fuel-flow-rate CW_f operating point on weighting factors derived by using corrected gage temperature CT_g as the argument of the steady-state model and for a 0.113-kilogram-per-second step in CW_f at the generalized external operating condition $v_k = v_2$ with both bleeds closed.

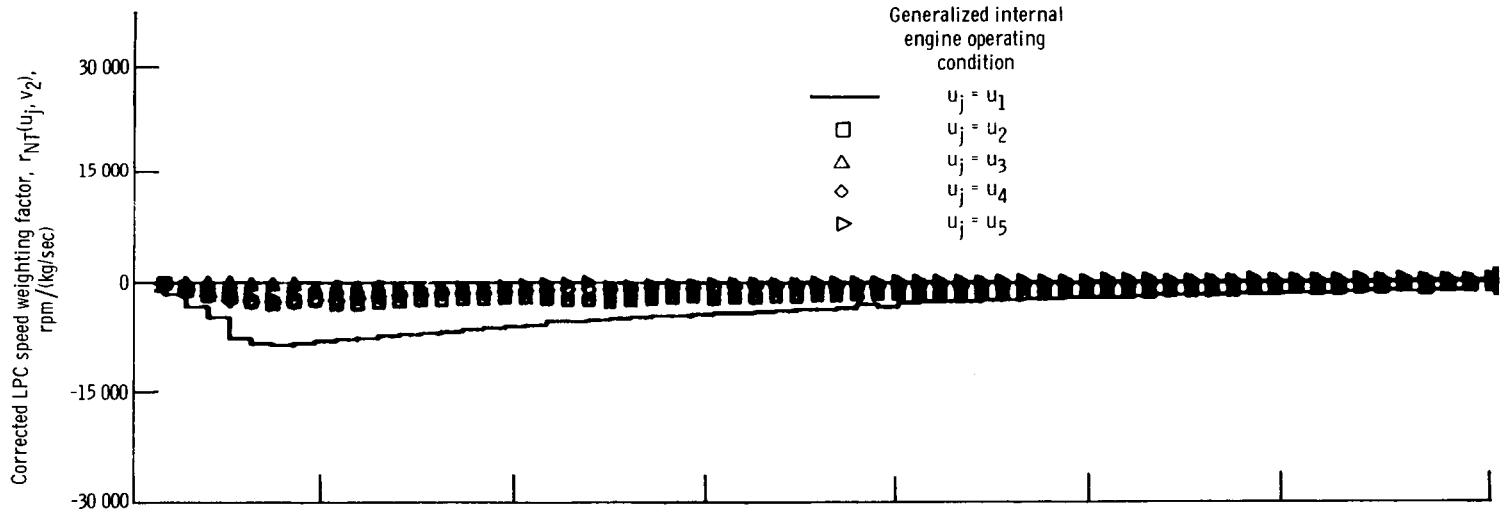

(c) Corrected low-pressure-compressor (LPC) speed $[y(n) = CN_L(n)]$.

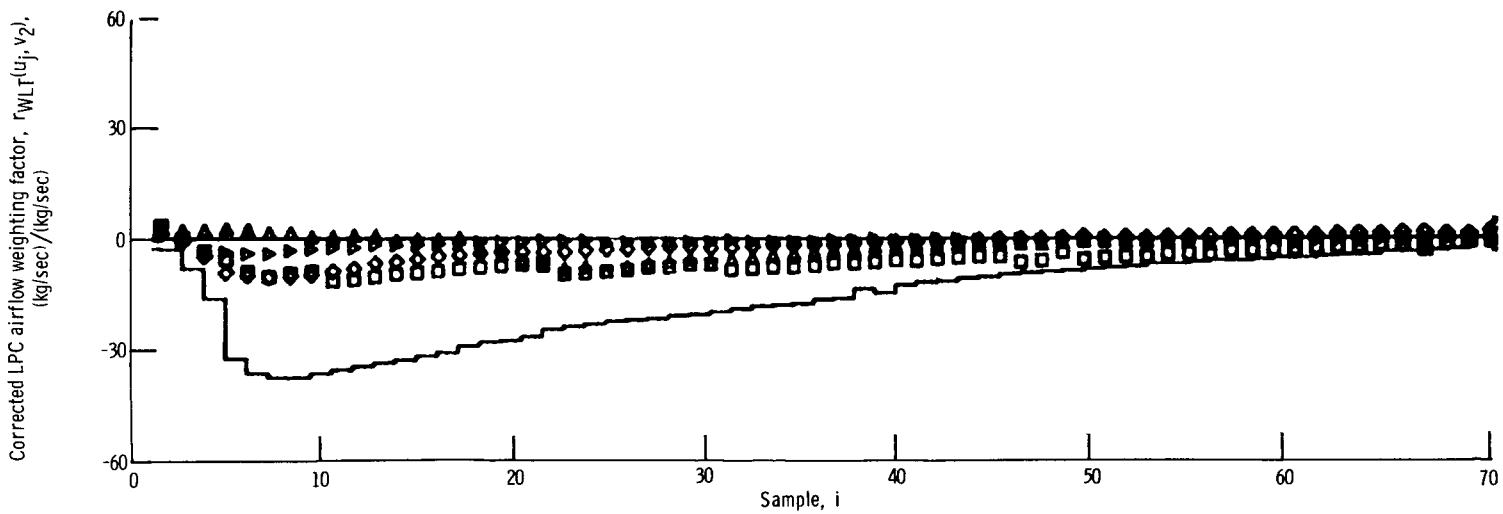

(d) Corrected low-pressure-compressor (LPC) airflow $[y(n) = CW_{A,L}(n)]$.

Figure 7. - Concluded.

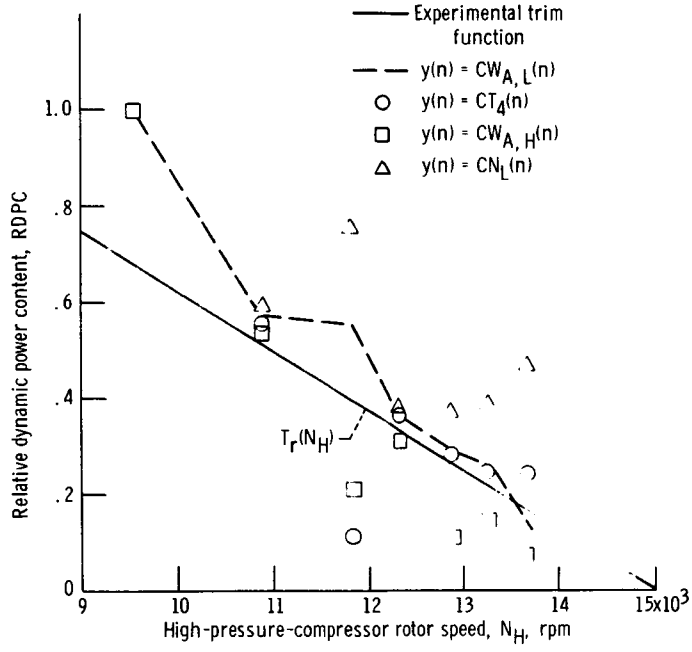

Figure 8. - Comparison of experimentally derived trim function with relative dynamic power content of various variables taken at external condition v_2.

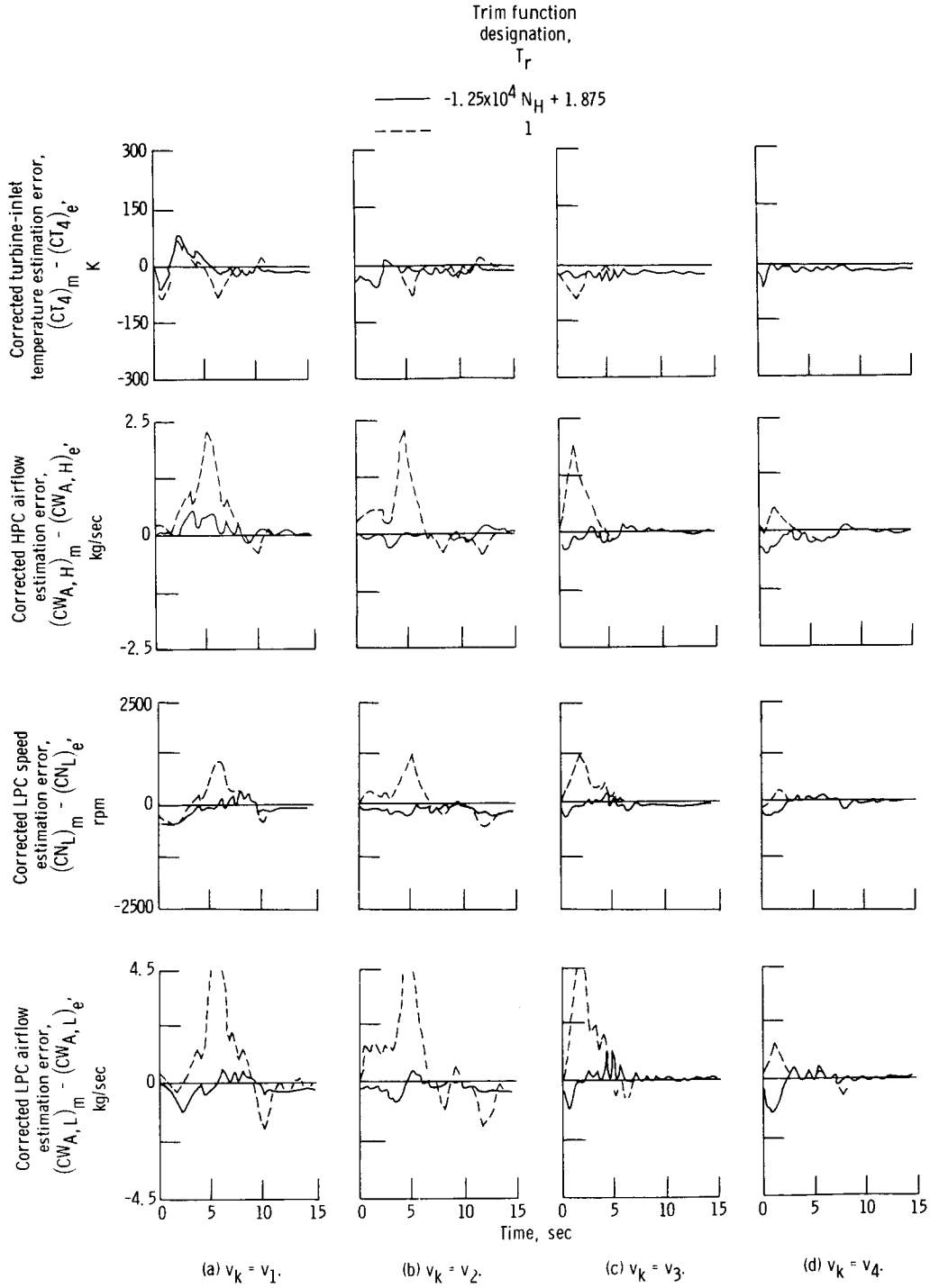

Figure 9. - Estimation error at selected external conditions v_k for models using corrected fuel flow rate CW_f as the argument of the steady-state term.

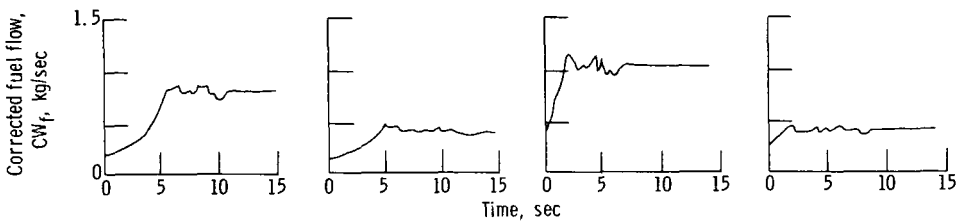

(a) $v_k = v_1$. (b) $v_k = v_2$. (c) $v_k = v_3$. (d) $v_k = v_4$.

Figure 10. - Fuel-flow-rate W_f transients due to a throttle step from idle to full augmentation with engine operating under bill-of-material control at selected external conditions v_k.

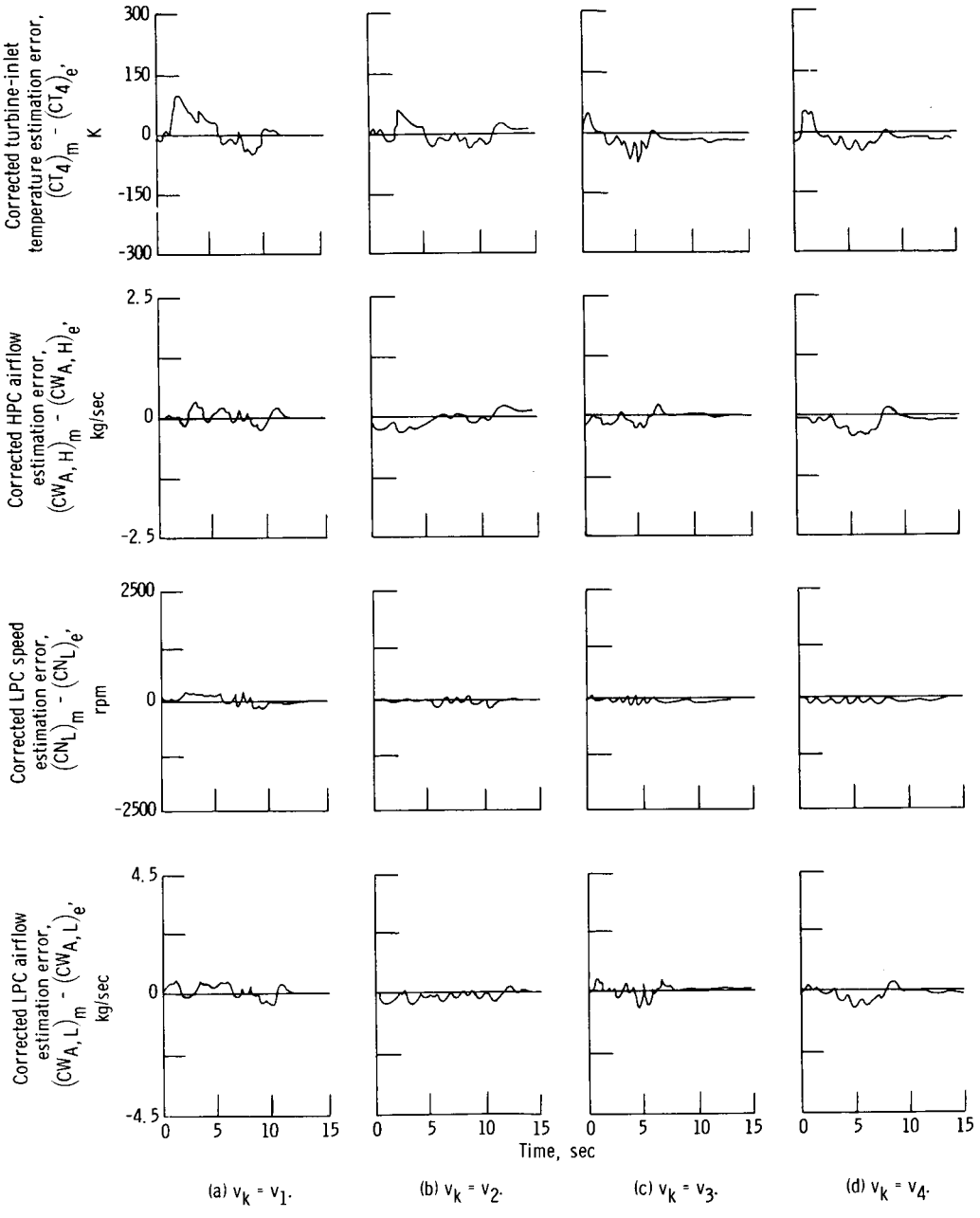

(a) $v_k = v_1$. (b) $v_k = v_2$. (c) $v_k = v_3$. (d) $v_k = v_4$.

Figure 11. - Estimation error at selected external conditions v_k for models using corrected low-pressure-compressor discharge static pressure $CP_{s,2.2}$ as the argument of the steady-state model.

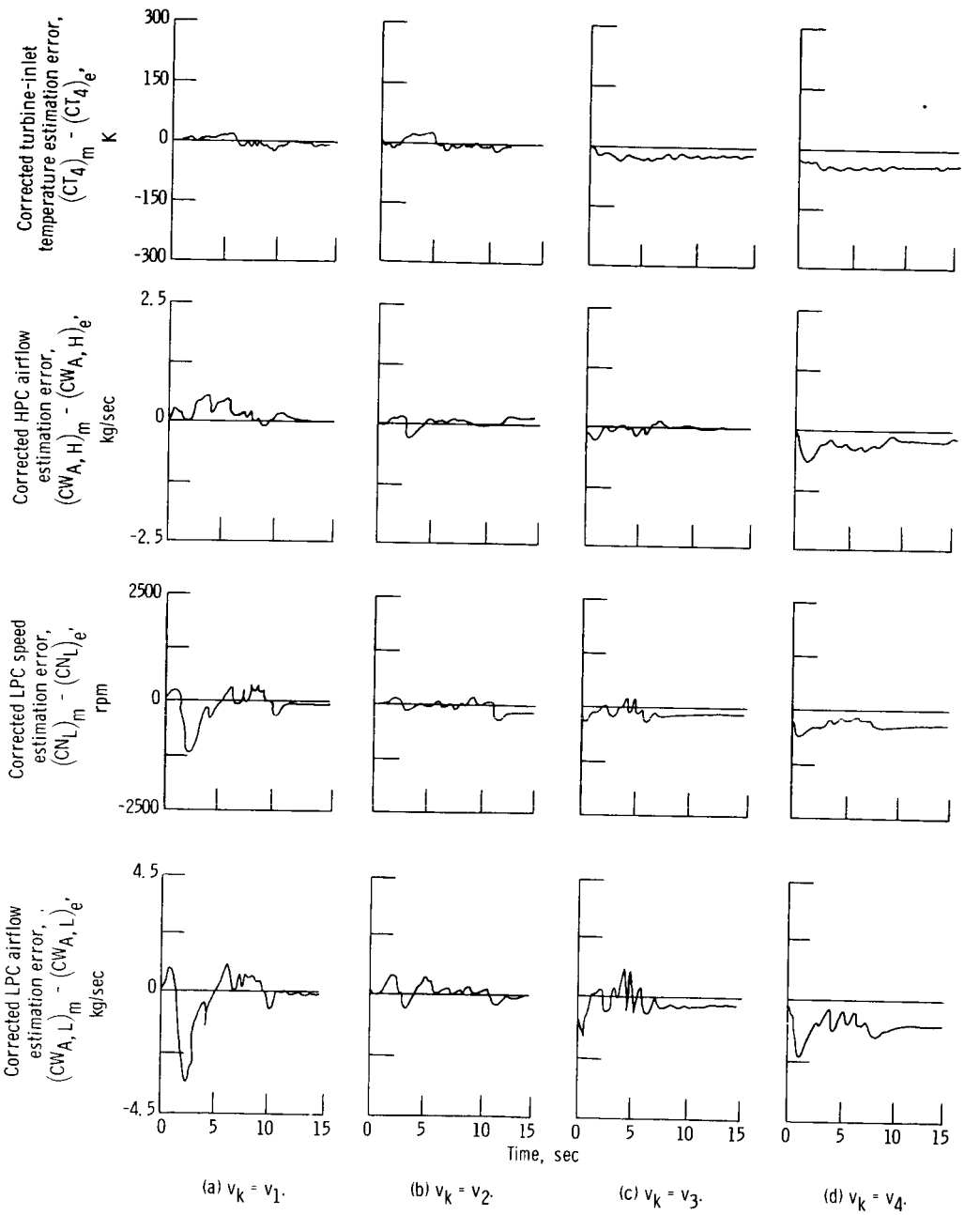

Figure 12. - Estimation error at selected external conditions v_k for models using corrected gage temperature CT_g as the argument of the steady-state term.

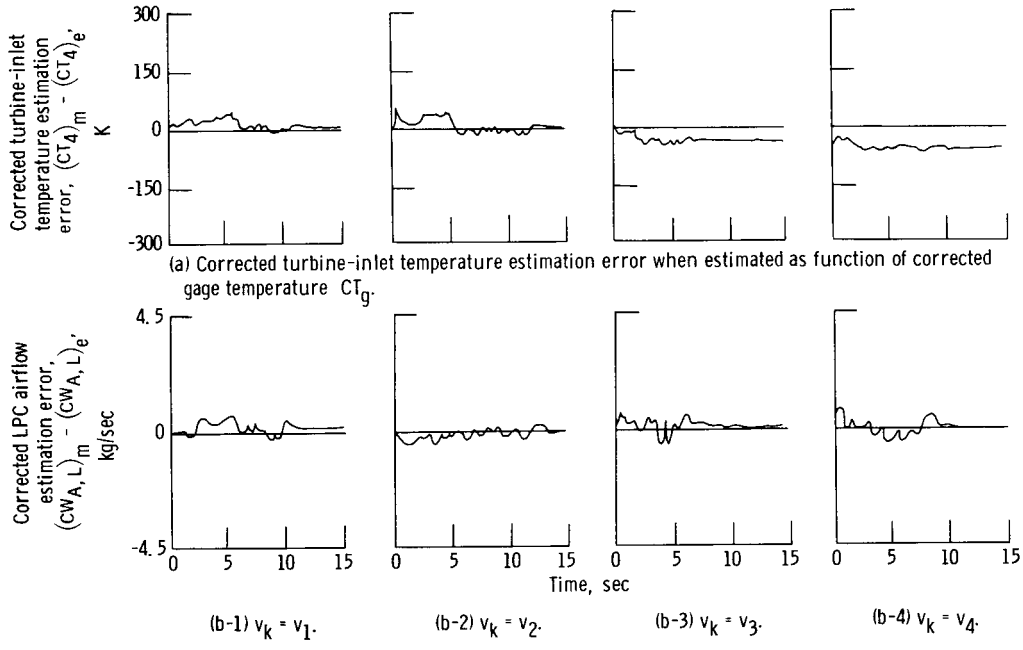

(a) Corrected turbine-inlet temperature estimation error when estimated as function of corrected gage temperature CT_g.

(b) Corrected low-pressure-compressor (LPC) airflow estimation error as function of corrected low-pressure-compressor (LPC) discharge static pressure $CP_{s,2.2}$.

Figure 13. - Estimation errors for steady-state models at selected external conditions v_k.

NASA-Langley, 1973 E-8560